MAGNETIC RESONANCE MICROIMAGING OF LIQUID WATER DISTRIBUTION IN SUGAR MAPLE WOOD BELOW FIBER SATURATION POINT

Roger E. Hernández*†

Professor

Claudia B. Cáceres

MSc Student
Centre de Recherche sur le Bois
Département des Sciences du Bois et de la Forêt
2425 rue de la Terrasse
Université Laval
Québec, QC, Canada, G1V 0A6

Abstract. Magnetic resonance (MR) microimaging was used to determine the distribution of liquid water in sugar maple wood (*Acer saccharum* Marsh.). Two moisture desorption tests were applied using saturated salt solutions at 21°C. Desorptions were accomplished between 58 and 96% RH starting from the full saturation state and from the FSP. Each moisture sorption condition at equilibrium was associated with a MR microimaging scan. Signal intensity (represented by false colors in the MR images) allowed visualization of the concentration of liquid water distributed into the wood structure. In most cases, the presence of liquid water was noticed in samples coming from the full saturation state at moisture contents below FSP. This result shows the coexistence of liquid and bound water even at moisture contents below the FSP. The remaining liquid water in the wood appears to be located principally in the lumina of the least accessible libriform fibers.

Keywords: Magnetic resonance microimaging, sugar maple, liquid water, fiber saturation point.

INTRODUCTION

The understanding of the hygroscopic behavior of wood is essential to achieve its optimal utilization. One of the most important features of wood hygroscopicity is the concept of the FSP because it governs the changes in different wood properties (Siau 1995). The FSP was first defined by Tiemann (1906) who established it as the moisture content at which the cell walls are saturated with bound water and the cell cavities have lost all liquid water. Many years later, studies on wood moisture sorption (Goulet and Hernández 1991; Hernández and Bizoň 1994; Hernández and Pontin 2006; Almeida and Hernández 2006a, 2006b) have questioned this concept of FSP. They reported the existence of a phenomenon called "hysteresis at saturation" that affects the moisture sorption of sugar maple wood above 63% RH (Goulet 1968; Hernández and Pontin 2006). This hysteresis implies that during desorption, the loss of bound water begins before all liquid water is removed from the wood.

Furthermore, Stamm (1964) added that the FSP is the moisture content at which physical properties such as swelling, shrinkage, and mechanical properties start to change. However, some studies that have associated moisture sorption tests at higher levels of RH with these properties (Hernández and Bizoň 1994; Hernández and Pontin 2006; Almeida and Hernández 2006a, 2006b) have shown that they began to change at equilibrium moisture contents (EMC) well above the FSP. Therefore, liquid water still remained in wood when the loss of bound water began. Almeida and Hernández (2006b) have suggested that the remaining liquid water could

* Corresponding author: Roger.Hernandez@sbf.ulaval.ca
† SWST member

be entrapped in cells associated with the smallest capillaries connecting the wood lumina. This could correspond to the openings of the simple pit membranes situated in the radial parenchyma cells given that these ray elements are considered as the least permeable flow paths in hardwoods (Wheeler 1982; Siau 1995).

The distribution and concentration of liquid water in wood tissues at different equilibrium sorption conditions are therefore fundamental points in the understanding of wood–water relationships. It has been demonstrated in this respect that ^{1}H nuclear magnetic resonance (NMR) is one of the most effective nondestructive methods for monitoring water movement (Hsi et al 1977; Riggin et al 1979; Brownstein 1980; Menon et al 1987; Flibotte et al 1990; Araujo et al 1992; Hartley et al 1994; Labbé et al 2006; Almeida et al 2007; Thygesen and Elder 2008).

In ^{1}H NMR, there are two different relaxation processes: spin–lattice relaxation (longitudinal relaxation), T_1, and spin–spin relaxation (transverse relaxation), T_2. The signal from water protons in wood cells can relax with different rates and can be easily divided into three principal components: solid wood, cell-wall water, and lumen water (Riggin et al 1979; Araujo et al 1993). Several ^{1}H NMR studies have shown the usefulness of spin–spin relaxation (T_2) for the characterization of water in wood (Riggin et al 1979; Brownstein 1980; Menon et al 1987, 1989; Flibotte et al 1990; Araujo et al 1992, 1993; Almeida et al 2007; Thygesen and Elder 2008). Moreover, it appears that T_2 relaxation is also sensitive to cell size, cell wall thickness, and wood cell proportions (Brownstein and Tarr 1979; Menon et al 1987, 1989; Flibotte et al 1990; Araujo et al 1993).

Most ^{1}H NMR experiments have been made using softwood species that have a simpler anatomical structure as compared with hardwoods. Thus, three different T_2 water populations have been differentiated: a fast T_2 that represents all cell-wall water, a medium T_2 that corresponds to water in earlywood lumina, and a slow T_2 that represents water in latewood lumina (Menon et al 1987; Flibotte et al 1990; Araujo et al 1992; Hartley et al 1994; Labbé et al 2006; Thygesen and Elder 2008). For hardwoods, there are four principal wood elements that can contain liquid water in their lumina: vessel elements, fibers, and axial and radial parenchyma. Nevertheless, their disposition, size distribution, and proportions are highly variable depending on species. Almeida et al (2007) carried out ^{1}H NMR measurements with two temperate hardwoods, sugar maple and beech, and one tropical hardwood, huayruro, at different equilibrium moisture contents. They observed three T_2 components: a slow T_2 that represents liquid water located in the lumina of the vessel elements, a medium T_2 that corresponds to liquid water located in the lumina of fiber and parenchyma elements, and a fast T_2 that represents bound or cell-wall water as found in softwoods. Their results also showed that, even at equilibrated conditions, liquid water was present at EMC values lower than the FSP. All liquid water was lost at 11.5% EMC for sugar maple, 11.4% EMC for beech, and 18% EMC for huayruro.

The next step is to achieve the visualization of this liquid water distribution in an image. Currently, magnetic resonance imaging (MRI) has become a reliable tool in wood imaging. MRI has been used to visualize the internal structure of wood (Hall and Rajanayagam 1986; Hall et al 1986; Cole-Hamilton et al 1995; Merela et al 2005; Oven et al 2008), evaluate water flow and distribution during drying (Olson et al 1990; MacMillan et al 2002; Meder et al 2003; Rosenkilde et al 2004), visualize moisture movement in wood composites (van Houts et al 2004, 2006), differentiate healthy tissue from decayed wood (Flibotte et al 1990; Kuroda et al 2006), and observe water drainage in wood (Almeida et al 2008). MRI is defined by different parameters that regulate the image quality permitting proper interpretation of the image characteristics. The image contrast depends on the variation of longitudinal relaxation time (T_1), transverse relaxation time (T_2), and proton density (water protons) in the sample. The effect

of these three factors is always present, but it is possible to emphasize one and minimize others to obtain a specific image contrast (Kastler 1997). The most important property in wood tissues for MRI is the water content. As the moisture content decreases, the signal intensity will be lower. In fact, as the proton density decreases, the T_2 values are faster and the signal is more difficult to obtain. However, the actual effect on the image intensity will depend on the imaging method and acquisition parameters (MacMillan et al 2002). The main objective of this work was to use MRI to visualize the distribution of liquid water in wood samples that were equilibrated during desorption at several moisture contents below the FSP.

MATERIALS AND METHODS

Experiments were carried out on sugar maple (*Acer saccharum* Marsh.) sapwood that was equilibrated in a conditioning room at 60% RH and 20°C. The samples were turned to obtain small 3.6-mm-dia cylinders (transverse to the grain) 20-mm long (parallel to the grain). The test material had an average basic wood density (oven-dry mass/green volume) of 556 kg/m^{-3} with a coefficient of variation of 2.5%.

Sorption Tests

The experiments consisted of moisture sorption tests combined with MR microimaging measurements. Fifty-four samples were prepared and distributed in nine matched groups. Five groups were destined for desorption experiments from full saturation. The other four groups were assigned to desorption experiments from the FSP. To avoid internal defects caused by fast adsorption, all samples were saturated using a mild procedure (Naderi and Hernández 1997; Almeida and Hernández 2007). All specimens were thus conditioned over a KCl-saturated salt solution (86% RH) for 10 da. The full saturation groups were then placed over distilled water for 10 da. The fiber saturation groups were also conditioned over distilled water until they achieved

the equilibrium condition after 16 da. Finally, the full saturation groups were immersed in distilled water until their maximum moisture content was reached by cycles of vacuum and atmospheric pressure.

All groups were then placed in sorption vats set at 21°C with a temperature control of ±0.01°C during extended periods (Hernández and Bizoň 1994). This permits a precise control of RH in the various desiccators serving as small sorption chambers. For each point of desorption, one desiccator containing six samples was used. One sample was used for the MR microimaging scan and the other five samples for EMC determination. All nine desorption conditions were carried out over saturated salt solutions in a single step procedure (Table 1). To determine equilibrium, the specimens were weighed periodically without being removed from the desiccators. Equilibrium was reached after at least 30 da of sorption. Once the EMC was reached, the first sample was placed into a 200-mm long, 5-mm outside diameter NMR sample tube. For better RH control during desorption, NMR tubes had been placed inside the desiccator at the beginning of the test. A Teflon dowel, 175-mm long and 4-mm dia, was then inserted in the tube to minimize the air space with which the wood could interact. A tight cap was used to seal the tube. Finally, the tube was placed in a 25-mm-thick Styrofoam box to minimize any change of hygrothermal conditions during transportation to the University of Montreal where the MR

Table 1. Characteristics of the moisture sorption conditions used in this experiment.

Sorption condition	State of sorption	Saturated salt solution	Nominal RH (%)
Equilibration at 21°C from full saturation state			
9	Desorption	K$_2$SO$_4$	96
8	Desorption	ZnSO$_4$	90
7	Desorption	KCl	86
6	Desorption	NaCl	76
5	Desorption	NaBr	58
Equilibration at 21°C from FSP			
4	Desorption	K$_2$SO$_4$	96
3	Desorption	ZnSO$_4$	90
2	Desorption	KCl	86
1	Desorption	NaCl	76

microimaging scans were made. The tube was weighed before transportation and at the beginning of the MR microimaging scan to detect any changes in moisture content.

Magnetic Resonance Microimaging Tests

[1]H MRI experiments were performed at 600 MHz on a 14.1-T Bruker Avance 600WB spectrometer equipped with a microimaging probe. The system was also equipped with three orthogonal field gradient coils permitting a maximum gradient of 30 G/mm along the z axis (ie parallel to the main magnetic field) and 20 G/mm in the x-y plane. A standard slice-selective spin-echo imaging sequence was used to acquire images of liquid water inside wood samples. Preliminary tests were made to select the best parameter configuration that permitted us to obtain a suitable quality image. A 1-mm-thick slice was selected by the use of sync-shaped selective pulses. Images were acquired using an accumulation of 1024 scans to obtain 100×100 pixel images with a field of view of 4 mm, leading to a nominal in-plane resolution of 40 μm. An echo time (TE) of 2.3 ms and a repetition time (TR) of 200 ms were used, leading to an experimental time of about 340 min for each image. All experiments were performed at 21°C.

Transverse and tangential images were obtained for each sorption condition. For the transverse image, the slice was selected at the middle of the longitudinal axis of each specimen. From this image, a perpendicular slice was taken at the middle to provide an image of the tangential–longitudinal plane of wood. The MR microimaging data acquisition, reconstruction, analysis, and visualization were made using ParaVision 4.0, Bruker's digital image processing software computer package. The intensity of the images was adjusted using the sample having the higher moisture content. This permitted us to visualize and compare the water concentration differences among the MR microimages. A color scale was chosen to obtain a clearer differentiation of the changes in signal intensity.

Environmental Scanning Electron Microscopy and Scanning Electron Microscopy Tests

The same specimens used for MR microimaging scans were cross-cut with a sharp circular saw at the same position where these scans were made (at the middle height). This freshly cut end-grain was then carefully cleaned with a razor blade mounted onto a microtome. This was done to match the MR microimages with the electron micrographs for comparison purposes. Environmental scanning electron microscopic (ESEM) pictures of end-grain surfaces were taken for each sample coming from the full saturation desorption test with a JEOL JSM6360LV microscope. Afterward, the same specimens were oven-dried for 2 h, mounted on standard aluminum stubs with silver paint, and coated with gold/palladium in a sputter-coater to obtain scanning electron microscopic (SEM) images using a JEOL 840-A microscope.

RESULTS AND DISCUSSION

Wood Hygroscopicity

The desorption curves of sugar maple wood obtained at 21°C are given in Fig 1. The upper curve at high RH corresponds to the boundary desorption (from full saturation) and the lower corresponds to desorption from FSP. In all cases, the standard errors of the EMC data do not exceed the symbol size shown. The difference between both curves at high RH is the result of the hysteresis at saturation phenomenon. Goulet and Hernández (1991) attributed such difference to the presence of liquid water during desorption. Several authors have confirmed this statement and relate it to the entrapment of liquid water in the most impermeable cells of wood, particularly radial parenchyma cells (Hernández and Bizoň 1994; Hernández and Pontin 2006; Almeida and Hernández 2006a, 2006b). These elements are considered as the least permeable flow paths in hardwoods (Wheeler 1982; Siau 1984). A paired Student's t-test was made to compare the EMC means

between the two desorption tests for each RH ($P = 0.05$). The results indicate that differences between EMC means were statistically significant for 96, 90, and 86% RH, although they were similar at 76% RH (Table 2). This could indicate that the entire loss of liquid water was already accomplished at 76% RH, which corresponds to approximately 17.2% EMC. This assumption will be confirmed later after examination of MR microimages of the samples.

The EMCs obtained in desorption starting from the full saturation state were also compared with those of previous studies performed on the same wood (Fig 2). Goulet (1968) and Hernández and Bizoň (1994) used larger samples of 15 (T) × 15 (L) × 45 (R) mm and 20 (R) × 20 (L) × 60 (T) mm, respectively. Their EMC values at

58% RH are similar with that obtained in the present work. At higher RH, the EMC values became increasingly different as RH increased. These differences would be almost entirely attributable to the amount of liquid water remaining in wood. Larger volumes of liquid water would remain entrapped in larger samples (Goulet 1968; Hernández and Bizoň 1994) than in smaller ones (Almeida et al 2007; present work). On the other hand, there were smaller differences in EMC between the results reported by Almeida et al (2007) and those of the present work, although both studies used a similar sample size but with different orientations. A radially oriented 4-mm-dia cylinder (L × T) and 20-mm long (R) was used by Almeida et al (2007). EMCs in these two studies were even different at 58% RH in which liquid water is virtually absent. Such differences
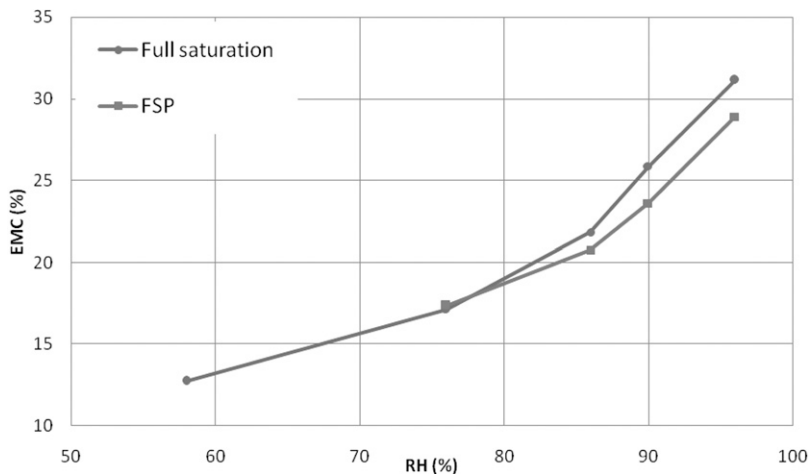
Figure 1. Equilibrium moisture content (EMC) as a function of RH for sugar maple wood at 21°C (standard errors did not exceed the symbol size).

Table 2.   Equilibrium moisture content as a function of RH at 21°C for different sample orientations of sugar maple wood.

RH (%)	Longitudinal[a]		Radial[a]		Tangential[a]	
	Desorption from		Desorption from		Desorption from	
	Full saturation (107.5%)	FSP (42.4%)	Full saturation (114.2%)	FSP (34.1%)	Full saturation (109.3%)	FSP (33.1%)
96	31.1 Aa[b]	28.9 Ba	31.6 Aa	28.2 Bb	31.7 Aa	27.5 Bc
90	25.9 Aa	23.6 Ba	25.9 Aa	23.8 Ba	25.6 Aa	23.3 Ba
86	21.8 Aa	20.7 Ba	22.4 Aab	21.5 Bb	22.7 Ab	21.5 Bb
76	17.1 Aa	17.4 Aa	17.5 Aa	17.5 Aa	17.6 Aa	17.0 Ba
58	12.7 a		13.1 a		12.8 a	

[a] Means of five replicates.
[b] Means within a row followed by the same letter are not significantly different at the $P = 0.05$ level. Uppercase letters are for desorption type comparison for each orientation separately. Lowercase letters are for orientation type comparison for each desorption type separately.
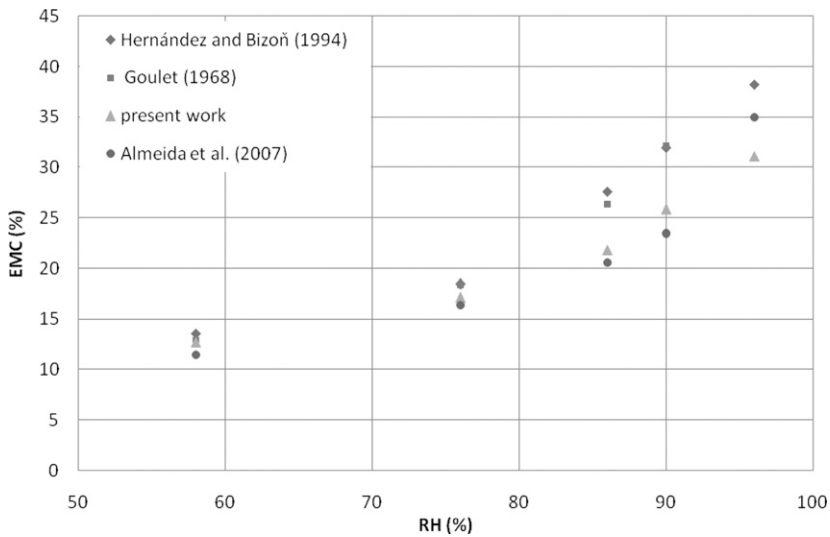
Figure 2. Comparison of equilibrium moisture content values of different studies obtained in desorption from full saturation state for sugar maple wood.

in desorption behavior could in part be explained by an eventual effect of the orientation of specimens on EMC. To test this hypothesis, an additional sorption test was carried out using samples 1) with their longer axis oriented following the rays; and 2) following the growth rings. Table 2 shows the EMC means and the means comparison test (unpaired Student's t test) obtained. Some statistically significant differences in EMC among orientations are shown. As discussed subsequently, water condensation occurred during the adsorption step over distilled water (during moisturizing wood up to FSP). Judging by the different nominal FSPs reached, this condensation was different for the three types of samples (Table 2). As a result, variable volumes of liquid water could even remain in the three types of samples at 96% RH. On the other hand, slight differences in EMC at 86% RH occurred between the longitudinal samples and the others. In contrast to the radial and tangential samples, longitudinal samples were taken from different pieces of wood, which can explain the differences in EMC. However, for most of the cases, the EMC values obtained for the three orientations were statistically similar. Therefore, the orientation of the sample does not appear to affect EMC. Differences in EMC between Almeida et al (2007) and

the present work must therefore be explained by other sources of variation.

Magnetic Resonance Microimaging Analysis

Previous ^{1}H NMR studies in wood have confirmed that analysis of the transverse relaxation times (T_2) permits the separation of water into three populations: bound water or cell-wall water with faster T_2; liquid water with medium T_2; and liquid water with slower T_2 (Menon et al 1987, 1989; Flibotte et al 1990; Araujo et al 1992, 1993; Almeida et al 2007). T_2 can also characterize water in different internal compartments because it is related to the size and proportion of woody tissues (Brownstein and Tarr 1979; Menon et al 1987; Araujo et al 1992; Almeida et al 2007). Thus, such results give a theoretical basis for the study of the distribution of water in wood by MRI at EMCs below the FSP.

Nevertheless, there are some limitations that should be considered when performing MRI analysis. First, the image intensity is dependent on the relationship among radiofrequency pulses, relaxation times (T_1 and T_2), and proton density (ρ) of water in the material of study

(Callaghan 1991). This relationship is described by the signal intensity equation:

$$S = \rho(1 - e^{(-TR/T_1)})(e^{(-TE/T_2)})$$

Olson et al (1990) have demonstrated that the image intensity is proportional to the quantity of liquid water present in the wood sample. Therefore, it is more difficult to obtain a clear image of wood at lower water concentrations. Another barrier is the size of the cells, because diameters smaller than 10 μm are difficult to observe with MRI (Köckenberger 2001). There are also some restrictions because of the MRI equipment and parameters used that will directly influence the quality of the image (MacMillan et al 2002; Bucur 2003; van Houts et al 2004).

As mentioned previously, the image intensity was set equally for each type of image to make them comparable. A color scale was also chosen to have a better contrast within the image. Colors varied from red, which shows the highest intensity (100%), to black that shows nil intensity (0%). The transposition of this to our results is as follows: from red to yellow indicates liquid water and from green to black indicates absence of liquid water. Thus, the limit intensity value

for detecting liquid water (yellow) was about 65% for transverse microimages and 58% for tangential microimages.

The MRI conditions used permitted us to obtain signal intensity that was mainly dependent on the liquid water concentration and the T_2 values. As discussed subsequently, images revealed primarily the variation in water proton density of the medium T_2 values. The signal of faster T_2 values was too low to be imaged.

Transverse and tangential MR microimages for the two desorption tests performed with the longitudinal oriented samples at two RH (96 and 86%) are shown in Figs 3-6. The EMC at 96% RH was 31.1% for desorption from full saturation (Fig 3a) and 28.9% for desorption conducted from FSP (Fig 3b). The difference between the two desorption experiments is 2.2% MC. The EMC value obtained from FSP should correspond exclusively to bound water. However, the adsorption step over distilled water gave a value of 42.4% MC (Table 2). According to previous research, the FSP of sugar maple should correspond to 31 or 30% (Hernández and Bizoň 1994; Hernández 2007). Condensation of water vapor apparently occurred, which implies that small volumes of
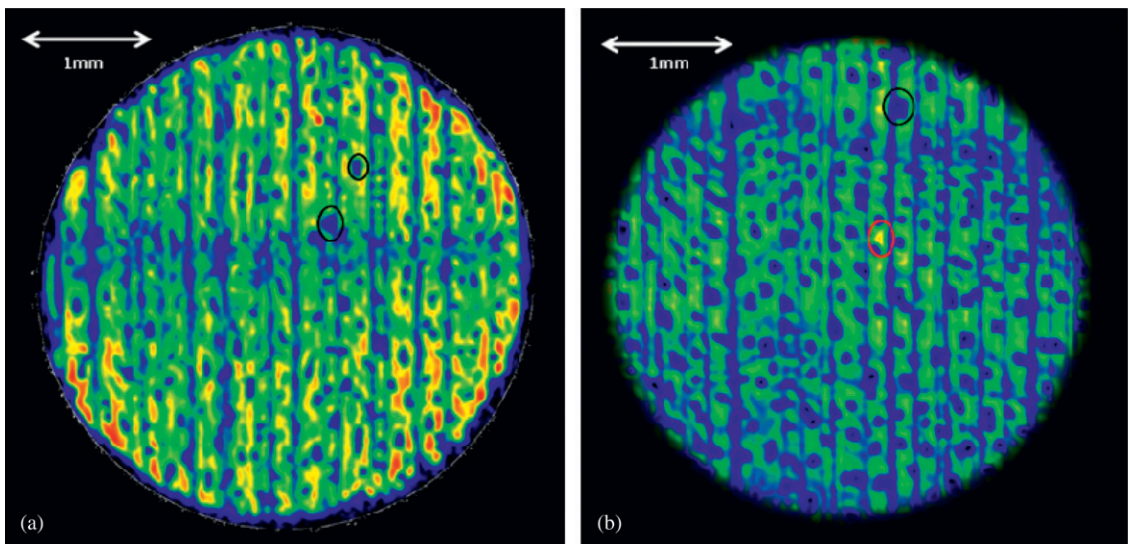
Figure 3. Magnetic resonance transverse microimages of the samples equilibrated at 96% RH. (a) From full saturation with an equilibrium moisture content (EMC) of 31.1%. (b) From FSP with an EMC of 28.9%.
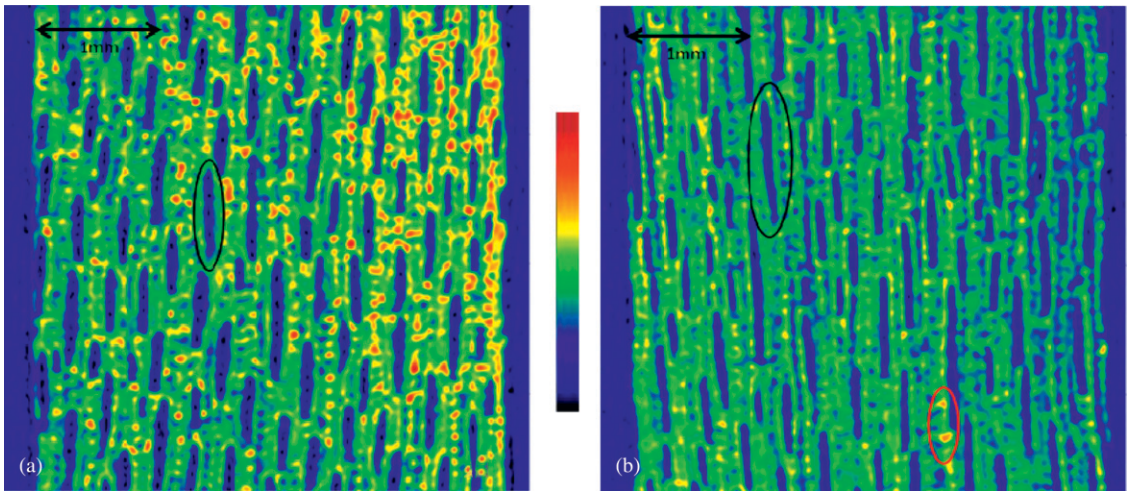
Figure 4.   Magnetic resonance tangential microimages of the samples equilibrated at 96% RH. (a) From full saturation with an equilibrium moisture content (EMC) of 31.1%. (b) From FSP with an EMC of 28.9%.
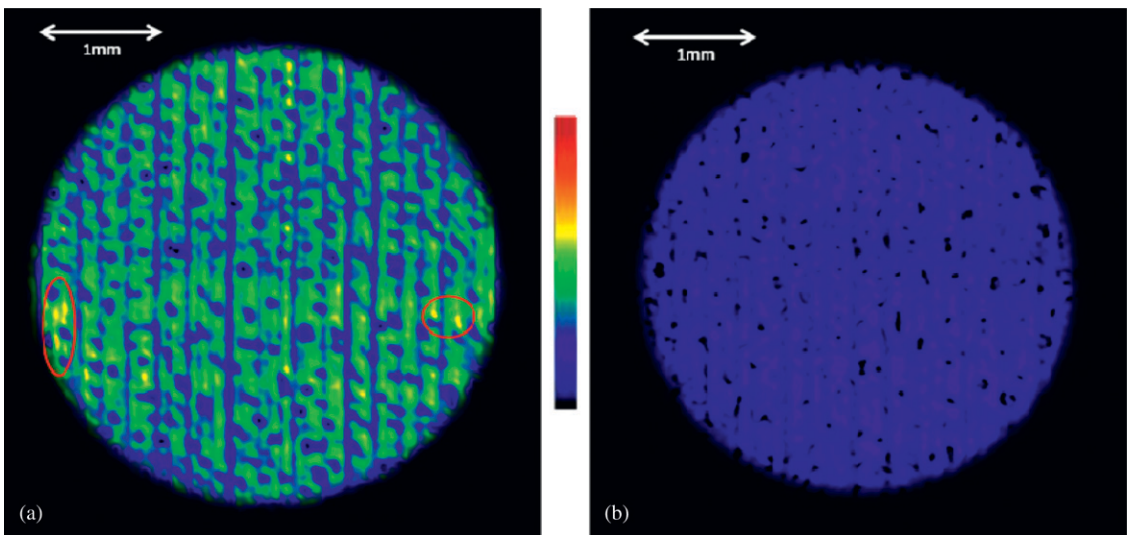
Figure 5.   Magnetic resonance transverse microimages of the samples equilibrated at 86% RH. (a) From full saturation with an equilibrium moisture content (EMC) of 21.8%. (b) From FSP with an EMC of 20.7%.

liquid water may be present in the sample coming from FSP desorption (Hernández 2007). This is confirmed by the fact that Figs 3b and 4b display some yellow–orange spots (red circles) revealing the presence of liquid water in the sample. Nevertheless, we can affirm that the difference in color between the two samples corresponds to the liquid water present in greater proportion in the specimens coming from full saturation (Figs 3a and 4a).

Figure 3a also illustrates (black circles) that all liquid water has been removed from the lumina of vessel elements at 96% RH. This early drainage of the pores in sugar maple has been described previously (Hernández and Bizoň 1994; Hernández and Pontin 2006; Almeida et al 2007). On other hand, liquid water appears to be located in the wood tissue surrounding the pores, because the colors red, orange, and yellow form
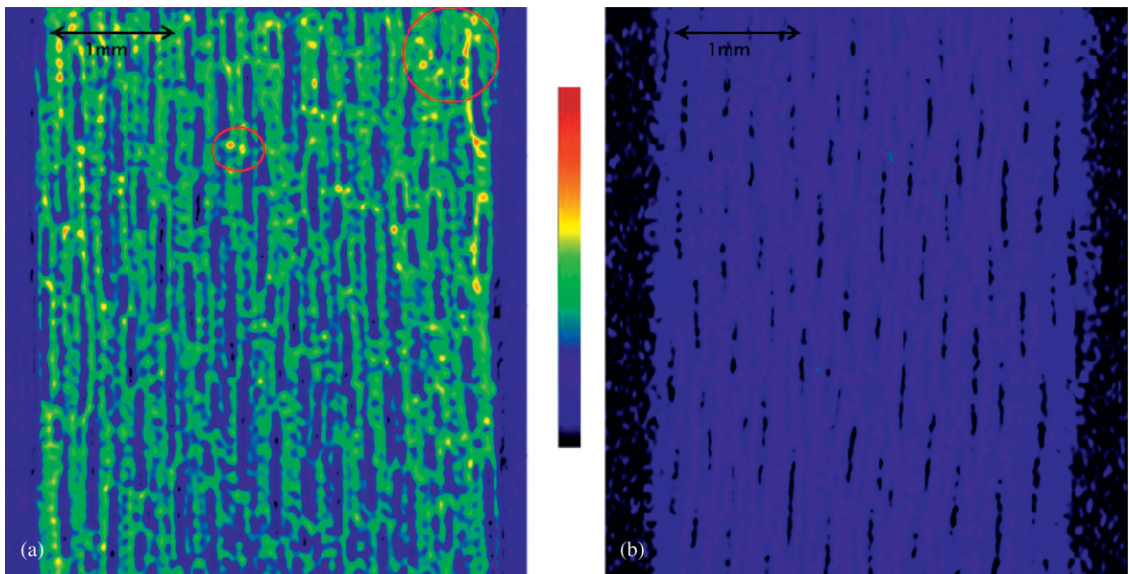
Figure 6. Magnetic resonance tangential microimages of the samples equilibrated at 86% RH. (a) From full saturation with an equilibrium moisture content (EMC) of 21.8%. (b) From FSP with an EMC of 20.7%.

irregular lines parallel to the rays. This exposes the fiber cavities as being the most likely location for liquid water. Moreover, the middle area of the sample seems to be devoid of liquid water because it shows mostly green and blue colors. This area corresponds to the limit of a growth ring, revealing it as an important flow path to drain liquid water in sugar maple.

As we could also see in Fig 3, Fig 4 shows more clearly that the rays are completely emptied of liquid water at 96% RH for both desorption tests (black circles). Considering the longitudinal and tangential-oriented samples, the maximum length of the rays was 4 mm, therefore liquid water needs to travel a maximum of 2 mm to be removed. For the radially oriented samples, the length of rays was 20 mm, and liquid water will need to travel a maximum of 10 mm to be removed. The distance for liquid water to leave the sample will depend on the orientation. However, Fig 4 shows the rays as one of the first elements to be drained of liquid water. Sugar maple has homocellular uniseriate and multiseriate rays (Panshin and de Zeeuw 1980). Carlquist (2007) found the existence of conspicuous bordered pits in the tangential walls of procum-

bent ray cells and fewer in their horizontal walls. This ray walls pitting would facilitate the flow of liquid water through ray cells. Moreover, ray-vessel pitting is similar to intervessel pitting in *Acer* species (Panshin and de Zeeuw 1980). The distance (size of the sample) used in these experiments should not be a barrier for the drainage of liquid water in ray elements. This observation contradicts previous hypotheses that established the lumina of radial parenchyma cells as the most probable location for the entrapment of liquid water below the FSP (Goulet and Hernández 1991; Hernández and Bizoň 1994). Figure 4a, however, shows that liquid water is located in the lumina of the fibers.

Figures 5a and 6a still show some liquid water (red circles) present at 86% RH that corresponds to 21.8% EMC. Figure 7a, however, does not depict liquid water at 76% RH, showing only blue and black colors. Thus, all remaining liquid water was removed at some point between these conditions. Almeida et al (2007) reported values of medium T_2 (liquid water) for sugar maple wood even at 76% RH (16.4% EMC). It is possible that the remnant of liquid water still present in wood at this level of RH might not
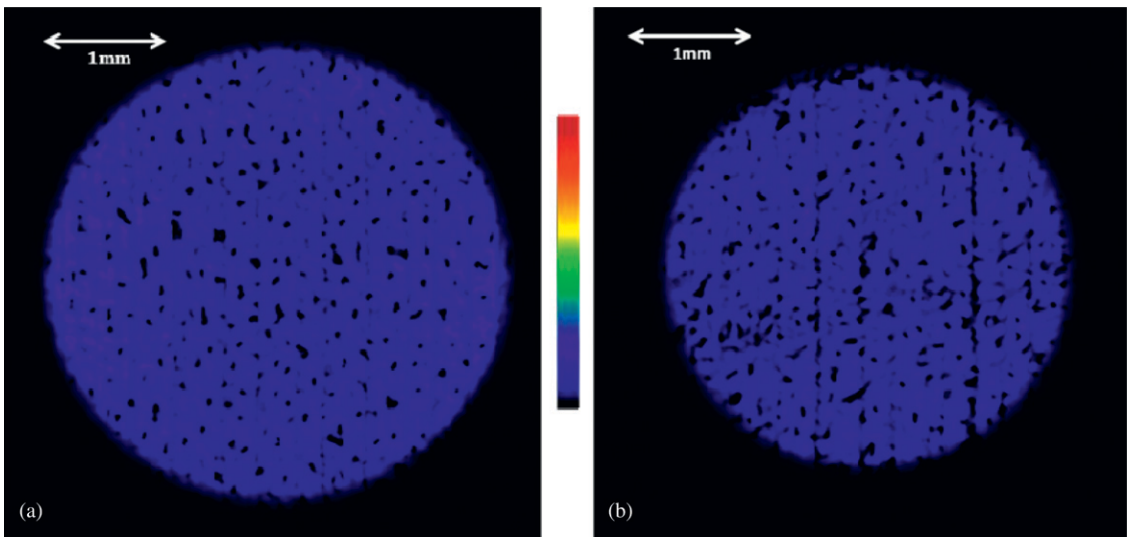
Figure 7.   Magnetic resonance transverse microimages of the samples equilibrated at 76% RH. (a) From full saturation with an equilibrium moisture content (EMC) of 17.1%. (b) From FSP with an EMC of 17.4%.

have been sufficient to produce a measurable signal using the parameters applied.

Figures 5b and 6b also illustrate that desorption from FSP at 86% RH (20.7% EMC) leaves no more liquid water, because their colors are only blue and black. Thus, all liquid water that had been present by water condensation had already been removed before attaining equilibrium at 86% RH. At 76% RH (Fig 7b) and 58% RH (not shown), both desorption tests were also devoid of liquid water.

Comparison of Magnetic Resonance Microimages and Scanning Electron Microscope Images

The comparison between MR microimages of the samples and the corresponding SEM images of the same sections showed very good agreement. SEM images provide higher resolution images of anatomical structure displayed in MR microimages. A typical comparison is presented in Fig 8 corresponding to the sample equilibrated at 96% RH from full saturation.

The higher concentration of liquid water (red to yellow spots) is found in the tissues outlying the

pores distributed all around the sample (Fig 8a). Hardwoods have two different types of fibers: libriform fibers that are elongated, commonly thick-walled cells with simple pits, and fiber tracheids that are commonly thick-walled cells with a small lumen, pointed ends and bordered pit pairs (IAWA 1964). The usual way to differentiate them is by their pitting. These two types of fibers represent approximately 61% of the total volume of sugar maple wood and their average length is about 0.92 mm (Panshin and de Zeeuw 1980). As mentioned previously, each pixel in the MR images represents 1-mm depth. Thus, Fig 8a could illustrate the behavior of one complete fiber with one tip of another fiber or two portions of two different fibers.

Carlquist (2001) established that in the evolution from tracheids to libriform fibers through the fiber tracheids, the pit membrane diameter and the borders of pits decrease and there are sequentially fewer pits. Thus, only fiber tracheids could take part in water transport, whereas libriform fibers will provide mechanical support. Cirelli et al (2008) established that fiber tracheids are part of the water-transport vessel system in sugar maple. Therefore, our hypothesis is that the liquid water entrapped in
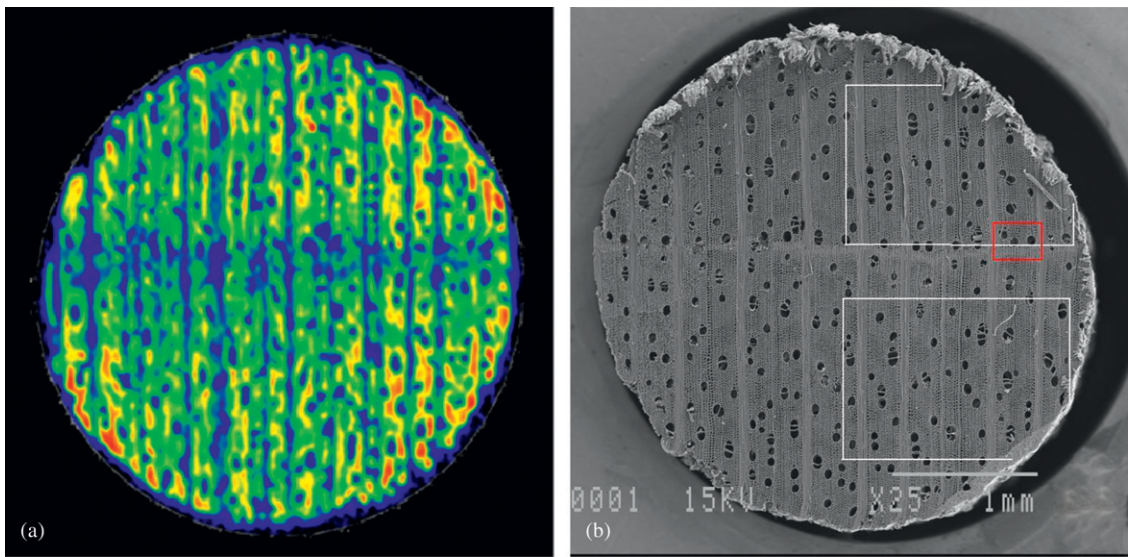
Figure 8. (a) Magnetic resonance transverse microimage of one sample equilibrated at 96% RH from full saturation (31.1% equilibrium moisture content). (b) Scanning electron microscopy image of the same section. The white lines indicate the position of Figs 9a and 9b. The red rectangle indicates the position of Fig 10.

wood at moisture contents below FSP is located in the libriform fibers, principally in those located far from the radial parenchyma and vessel elements.

According to Vazquez-Cooz and Meyer (2006), most libriform fibers in sugar maple have simple pits with elliptical shapes that are grouped mainly near the center of the fiber. Thus, their extremities do not have communication between cells. In contrast, pits in the fiber tracheids are rather evenly distributed along the fiber length. Furthermore, Magendans and van Veenendaal (1999) stated that complementary pits in neighboring walls of adjacent libriform fibers are not in perfect alignment as are the complementary pits of fiber tracheid pit pairs. Cirelli et al (2008) found no pits or only blind pits connecting libriform fibers to vessels and no connections between libriform fibers and fiber tracheids. Fiber-to-fiber simple pit pairs were scarce in sugar maple. Therefore, libriform fibers appear to be more isolated from the other cell groups.

Libriform fibers have also larger lumina than fiber tracheids and have intercellular spaces that occur in various patterns, ranging from large groups to wavy bands (Vazquez-Cooz and Meyer 2006). More recently, Vazquez-Cooz and Meyer (2008) have discarded the use of the terms libriform fibers and fiber tracheids for fiber type 1 and 2, respectively. The IAWA Committee (1989) considers these terms as corresponding to different subtypes of libriform fibers.

Figure 9 shows two sections of wood sample presented in Fig 8, which show fibers with different lumen sizes. Good agreement exists between the distribution of the larger lumen fibers in Figs 9a and 9b and the distribution of the liquid water in Fig 8a. Therefore, it is possible to establish that liquid water is entrapped principally in the libriform fibers, probably at their lumina extremities. Furthermore, liquid water could also be present to some extent in the intercellular spaces, which are commonly associated with libriform fibers (Vazquez-Cooz and Meyer 2006). The connections between intercellular spaces and surrounding cells have not yet been studied.

This analysis could help in the interpretation of the EMC differences between previous studies

(Goulet 1968; Hernández and Bizoň 1994; Almeida et al 2007). As mentioned previously, such differences in EMC could be entirely because of the quantity of liquid water in the sample such that larger samples could entrap more liquid water than smaller ones. Thus, the longer the longitudinal axis in the sample, the higher the possibility of capturing liquid water, which will also increase if the sample has a larger section (R × T). Goulet (1968) and Hernández and Bizoň (1994) used larger samples than those used in the present work. Larger samples give them a greater probability to lose the connectivity among wood cells and consequently entrap more liquid water. However, differences can also be attributed to the great variability in the proportion and distribution of fiber tracheids and libriform fibers. Panshin and de Zeeuw (1980) have stated that they vary between species, among individuals of the same species, and within a tree.

Figure 8b clearly shows the limit of one growth ring that represents a region without liquid water in Fig 8a. That area appears to be formed by fiber tracheids because they have smaller lumina (Fig 10). Sparse marginal parenchyma could also be present as occasional cells (Panshin and de Zeeuw 1980). Cirelli et al (2008) have found a good association between fiber tracheids and vessels connected through bordered pit pairs. A large pore distribution is also present along the limit of the growth ring that could indicate an easy passage for liquid water between the fiber tracheids and vessels (Fig 8b).

SUMMARY AND CONCLUSIONS

The MR microimaging technique was used to obtain images of liquid water distribution in sugar maple wood at equilibrium moisture contents below the FSP. Desorption experiments from FSP and from full saturation desorption were carried out at 21°C to distinguish the location of liquid water in the wood structure.
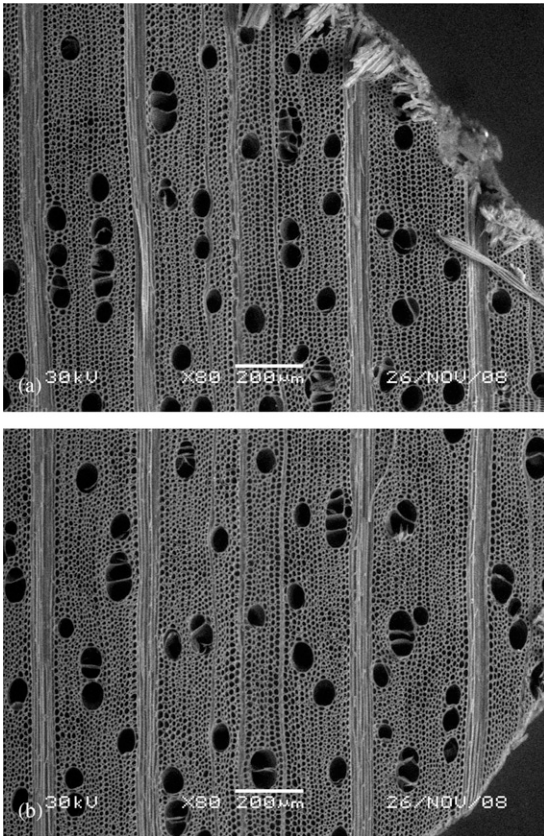
Figure 9. Environmental scanning electron microscopy transverse images of two different sections of the sample (a and b) equilibrated at 96% RH (31.1% equilibrium moisture content) from full saturation.
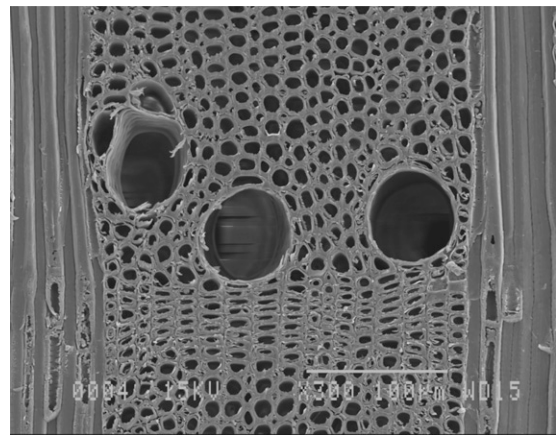
Figure 10. Scanning electron microscopy transverse image of the limit of growth ring of the sample equilibrated at 96% RH (31.1% equilibrium moisture content) from full saturation.

The principal conclusions are listed subsequently:

1. Liquid water was found below FSP even at equilibrated conditions. Thus, there is a loss of bound water even when liquid water is entrapped in wood. The concept of FSP should be re-evaluated.
2. MR microimaging is a technique that lends itself as a powerful tool to visualize liquid water distribution over a wide range of moisture contents.
3. MR microimages show good evidence that vessel and ray elements are drained of liquid water before achieving equilibration at 96% RH.
4. MR microimages, and ESEM and SEM images, suggest that the remaining liquid water below FSP could be principally entrapped toward the ends of the libriform fibers given that pits in these elements are predominantly concentrated toward their centers. Remnants of liquid water could also be located in the intercellular spaces present in this wood.

ACKNOWLEDGMENTS

REFERENCES

Almeida G, Gagné S, Hernández RE (2007) A NMR study of water distribution in hardwoods at several equilibrium moisture contents. Wood Sci Technol 41(4):293-307.

Almeida G, Hernández RE (2006a) Changes in physical properties of tropical and temperate hardwoods below and above the fiber saturation point. Wood Sci Technol 40(7):599-613.

Almeida G, Hernández RE (2006b) Changes in physical properties of yellow birch below and above the fiber saturation point. Wood Fiber Sci 38(1):74-83.

Almeida G, Hernández RE (2007) Dimensional changes of beech wood resulting from three different re-wetting treatments. Holz Roh Werkst 65(3):193-196.

Almeida G, Leclerc S, Perré P (2008) NMR imaging of fluid pathways during drainage of softwood in a pressure membrane chamber. Int J Multiph Flow 34(3):312-321.

Araujo CD, MacKay AL, Hailey JRT, Whittall KP, Le H (1992) Proton magnetic resonance techniques for characterization of water in wood: Application to white spruce. Wood Sci Technol 26(2):101-113.

Araujo CD, MacKay AL, Whittall KP, Hailey JRT (1993) A diffusion model for spin–spin relaxation of compartmentalized water in wood. J Magn Reson B 101(3):248-261.

Brownstein KR (1980) Diffusion as an explanation of observed NMR behavior of water absorbed on wood. J Magn Reson 40(3):505-510.

Brownstein KR, Tarr CE (1979) Importance of classical diffusion in NMR studies of water in biological cells. Phys Rev A 19(6):2446-2453.

Bucur V (2003) Techniques for high resolution imaging of wood structure: A review. Meas Sci Technol 14(12): R91-R98.

Callaghan PT (1991) Principles of nuclear magnetic resonance microscopy. Oxford University Press, Oxford, UK. 492 pp.

Carlquist S (2001) Comparative wood anatomy: Systematic, ecological, and evolutionary aspects of dicotyledon wood. Springer-Verlag, Berlin, Germany. 448 pp.

Carlquist S (2007) Bordered pits in ray cells and axial parenchyma: The histology of conduction, storage, and strength in living wood cells. Bot J Linn Soc 153(2): 157-168.

Cirelli D, Jagels R, Tyree MT (2008) Toward an improved model of maple sap exudation: The location and role of osmotic barriers in sugar maple, butternut and white birch. Tree Physiol 28(8):1145-1155.

Cole-Hamilton DJ, Kaye B, Chudek JA, Hunter G (1995) Nuclear magnetic resonance imaging of waterlogged wood. Stud Conserv 40(1):41-50.

Flibotte S, Menon RS, MacKay AL, Hailey JR (1990) Proton magnetic resonance of western red cedar. Wood Fiber Sci 22(4):362-376.

Goulet M (1968) Phénomènes de second ordre de la sorption d'humidité dans le bois au terme d'un conditionnement de trois mois à temperature normale. Second partie: Essais du bois d'érable en compression radiale. Note de recherche N°3. Département d'exploitation et utilisation des bois de l'Université Laval, Québec, Canada. 30 pp.

Goulet M, Hernández RE (1991) Influence of moisture sorption on the strength of sugar maple wood in tangential tension. Wood Fiber Sci 23(2):197-206.

Hall LD, Rajanayagam V (1986) Evaluation of the distribution of water in wood by use of three dimensional proton NMR volume imaging. Wood Sci Technol 20(4):329-333.

Hall LD, Rajanayagam V, Stewart WA, Steiner PR (1986) Magnetic resonance imaging of wood. Can J For Res 16(2):423-426.

Hartley ID, Kamke FA, Peemoeller H (1994) Absolute moisture content determination of aspen wood below the

fiber saturation point using pulsed NMR. Holzforschung 48(6):474-479.

Hernández RE (2007) Effects of extraneous substances, wood density and interlocked grain on fiber saturation point of hardwoods. Wood Mater Sci Eng 2(1):45-53.

Hernández RE, Bizoň M (1994) Changes in shrinkage and tangential compression strength of sugar maple below and above the fiber saturation point. Wood Fiber Sci 26(3):360-369.

Hernández RE, Pontin M (2006) Shrinkage of three tropical hardwoods below and above the fiber saturation point. Wood Fiber Sci 38(3):474-483.

Hsi E, Hossfeld R, Bryant RG (1977) Nuclear magnetic resonance relaxation study of water absorbed on milled northern white cedar. J Colloid Interface Sci 62(3):389-395.

IAWA (1964) Multilingual glossary of terms used in wood anatomy. Committee on Nomenclature. International Association of Wood Anatomists. Verlagsanstalt Buchdruckerei Konkordia, Winterthur, Switzerland. 186 pp.

IAWA Committee (1989) IAWA list of microscopic features for hardwood identification with an appendix on non-anatomical information. IAWA Bull 10(3):219-332.

Kastler B (1997) Comprendre l'IRM: Manuel d'auto-apprentissage. Masson, Paris, France. 232 pp.

Köckenberger W (2001) Nuclear magnetic resonance micro-imaging in the investigation of plant cell metabolism. J Exp Bot 52(356):641-652.

Kuroda K, Kanbara Y, Inoue T, Ogawa A (2006) Magnetic resonance micro-imaging of xylem sap distribution and necrotic lesions in tree stems. IAWA J 27(1):3-17.

Labbé N, De Jéso B, Lartigue J-C, Daudé G, Pétraud M, Ratier M (2006) Time-domain ^{1}H NMR characterization of the liquid phase in greenwood. Holzforschung 60(3):265-270.

MacMillan MB, Schneider MH, Sharp AR, Balcom BJ (2002) Magnetic resonance imaging of water concentration in low moisture content wood. Wood Fiber Sci 34(2):276-286.

Magendans JFC, van Veenendaal WLH (1999) Bordered pits and funnel pits: Further evidence of convergent evolution. Wag Ag Un P 99(2):31-97.

Meder R, Codd SL, Franich RA, Callaghan PT, Pope JM (2003) Observation of anisotropic water movement in Pinus radiata D. Don sapwood above fiber saturation using magnetic resonance micro-imaging. Holz Roh Werkst 61(4):251-256.

Menon RS, Mackay AL, Flibotte S, Hailey JRT (1989) Quantitative separation of NMR images of water in wood on the basis of T_2. J Magn Reson 82(1):205-210.

Menon RS, MacKay AL, Hailey JRT, Bloom M, Burgess AE, Swanson JS (1987) An NMR determination of the physio-

logical water distribution in wood during drying. J Appl Polym Sci 33(4):1141-1155.

Merela M, Sepe A, Oven P, Sersa I (2005) Three-dimensional in vivo magnetic resonance microscopy of beech (Fagus sylvatica L.) wood. Magn Reson Mater Phy 18(4):171-174.

Naderi N, Hernández RE (1997) Effect of re-wetting treatment on the dimensional changes of sugar maple wood. Wood Fiber Sci 29(4):340-344.

Olson JR, Chang SJ, Wang PC (1990) Nuclear magnetic resonance imaging: A noninvasive analysis of moisture distributions in white oak lumber. Can J Res 20(5):586-591.

Oven P, Merela M, Mikac U, Serša I (2008) 3D magnetic resonance microscopy of a wounded beech branch. Holzforschung 62(3):322-328.

Panshin AJ, de Zeeuw C (1980) Textbook of wood technology. McGraw-Hill, New York, NY. 772 pp.

Riggin MT, Sharp AR, Kaiser R, Schneider MH (1979) Transverse NMR relaxation of water in wood. J Appl Polym Sci 23(11):3147-3154.

Rosenkilde A, Gorce JP, Barry A (2004) Measurement of moisture content profiles during drying of Scots pine using magnetic resonance imaging. Holzforschung 58(2):138-142.

Siau JF (1984) Transport processes in wood. Springer-Verlag, Berlin, Germany. 245 pp.

Siau JF (1995) Wood: Influence of moisture on physical properties. Virginia Tech, Blacksburg, VA. 227 pp.

Stamm AJ (1964) Wood and cellulose science. Ronald Press, New York, NY. 549 pp.

Thygesen LG, Elder T (2008) Moisture in untreated, acetylated, and furfurylated Norway spruce studied during drying using time domain NMR. Wood Fiber Sci 40(3):309-320.

Tiemann HD (1906) Effect of moisture upon the strength and stiffness of wood. USDA For Serv, Bull 70, Government Printing Office, Washington, DC. 144 pp.

van Houts JH, Wang SQ, Shi HP, Kabalka GW (2006) Moisture movement and thickness swelling in oriented strandboard, part 2: Analysis using a nuclear magnetic resonance imaging body scanner. Wood Sci Technol 40(6):437-443.

van Houts JH, Wang SQ, Shi HP, Pan HJ, Kabalka GW (2004) Moisture movement and thickness swelling in oriented strandboard, part 1: Analysis using nuclear magnetic resonance microimaging. Wood Sci Technol 38(8):617-628.

Vazquez-Cooz I, Meyer RW (2006) Distribution of libriform fibers and presence of spiral thickenings in fifteen species of Acer. IAWA J 27(2):173-182.

Vazquez-Cooz I, Meyer RW (2008) Fundamental differences between two fiber types in Acer. IAWA J 29(2):129-141.

Wheeler EA (1982) Ultrastructural characteristics of red maple (Acer rubrum L.) wood. Wood Fiber Sci 14(1):43-53.